Taraka V. Pattela, Leonardo Disperati*, Enrico D'Addario and Daniele Rappuoli

Multi-temporal GNSS, RTS, and InSAR for very slow-moving landslide displacement analysis

https://doi.org/10.1515/jag-2025-0029
Received February 19, 2025; accepted March 17, 2025;
published online May 23, 2025

Abstract: Very slow-moving landslides threaten infrastructures and safety, yet detecting their subtle, long-term displacements remains challenging. The eastern slope of Mount Amiata, Tuscany, Italy, where high-precision geodetic monitoring is required to control the very slow-moving landslides affecting the area, represents an example of this issue. Namely, in this study we assess whether the joint exploitation of multi-temporal GNSS (continuous and periodic), Robotic Total Stations (RTS), and Persistent Scatterer InSAR techniques allows us to provide a coherent picture of very slow-moving landslide areas. While GNSS provides useful long-term displacement data, it may be affected by low signal-to-noise ratio, limiting precision to cm-mm level. Hence, to refine the outputs, we implement statistical time-series analysis, including weighted linear regression and 95 % confidence intervals. RTS delivered high-precision 3D data associated to local-scale measurements, while InSAR extended coverage to wider areas, resolving East-West and Vertical components from Sentinel-1 data. We highlight that, since 2019, the monitoring network has recorded horizontal displacements of *ca.* 10–15 mm/year, while vertical movements reached −7 mm/year, well correlating with local morphology and bedrock geology characteristics. We also perform a comparison of GNSS and RTS measurements with InSAR datasets, highlighting the limitations of InSAR in vegetated and geometrically complex terrains, while also confirming its value in capturing large scale displacement trends. The findings demonstrate that, despite their individual limitations, the joint exploitation of GNSS, RTS, and InSAR allow to provide a comprehensive framework for very slow-moving landslide areas. The scalable, cost-effective multi-source system here developed represents a robust approach for monitoring very slow-moving landslides, supporting risk mitigation strategies in landslide-prone regions.

Keywords: very slow-moving landslides; GNSS; RTS; PSInSAR; statistical time-series analysis

1 Introduction

Very slow-moving landslides, characterised by displacement rates less than *ca.* 16 mm/year [1] pose significant long-term risks to urban infrastructures. While these landslides may not cause an immediate threat, their cumulative effects over time can result in increased risk, particularly in geologically complex areas [2]. Monitoring such slope movements is crucial for hazard-risk mitigation and understanding the evolution of displacement rates [3, 4]. Accurate monitoring of very slow-moving landslides requires systems capable of detecting mm-scale movements for extended periods. Over the years, various geodetic techniques have been employed to measure surface displacements, each one with strengths and limitations. Tools such as crack meters [5] and clinometers [6] are effective mainly for localized small-scale applications where rock outcrops or infrastructures are involved. Robotic Total Station (RTS) provides high-resolution, accurate measurements [7] but it is limited by topographic and visibility challenges. Broader spatial coverage and regional scale displacement measurements have been achieved using GNSS and InSAR, with GNSS providing precise displacement monitoring and flexible acquisition styles, while InSAR may achieve mm-level precision over extensive areas [8, 9]. Despite advancements, significant challenges remain in order to model the displacement rates of very slow-moving landslides. This study investigates the displacement dynamics of a landslide area affecting infrastructures on the eastern slope of the Mount Amiata volcano, Tuscany, Italy. By exploiting together multi-temporal GNSS measurements (both continuous and periodic), RTS and InSAR data, we map spatio-temporal displacement trends. This paper presents the monitoring strategies, time-series analysis methods, and findings, offering valuable insights

***Corresponding author: Leonardo Disperati**, Department of Earth, Environmental and Physical Sciences, University of Siena, Siena, Italy, E-mail: disperati@unisi.it. https://orcid.org/0000-0001-6510-2575
Taraka V. Pattela and Enrico D'Addario, Department of Earth, Environmental and Physical Sciences, University of Siena, Siena, Italy, E-mail: taraka.pattela@unisi.it (T.V. Pattela), enrico.daddario@unisi.it (E. D'Addario). https://orcid.org/0000-0002-6057-5418 (T.V. Pattela)
Daniele Rappuoli, Unione dei Comuni Amiata Val d'Orcia, Piancastagnaio, Italy, E-mail: d.rappuoli@uc-amiatavaldorcia.si.it

and demonstrating the effectiveness of the multi-sources geodetic approach for mm-level monitoring of very slow-moving landslides.

2 Study area

Mount Amiata (1,731 m a.s.l.) is a Pleistocene volcanic edifice with activity dated to approximately 305–231 ky, emplaced during the late extensional phase of the Northern Apennines orogenesis [10, 11]. The edifice is made up of trachydacitic and olivine-latitic lava flows and domes [10, 12], often weathered to saprolite [13] and corestones [14, 15]. The volcanic rocks unconformably overlie the Ligurian Units (Jurassic – Eocene) composed of clay-rich sedimentary and ophiolitic rocks [10]. This stratigraphic framework has led to development of widespread landslides and deep-seated gravitational slope deformations along the slopes of Mount Amiata [16]. The study area is located in the Abbadia San Salvatore town, eastern slope of Mount Amiata (Figure 1), where a slow-moving landslide affects the main road (Via Remedi) connecting the southern sector of the volcanic area, the neighboring buildings and the downslope area. Here (Figure 1a), the contact between the volcanic rocks of the Quaranta Formation (QRT) and the underlying shales with calcareous interlayers of the Santa Fiora Formation (SIL, Ligurian Units) is observed. The field surveys conducted before installing the monitoring system allowed us to recognize, uphill Via Remedi, the landslide main escarpment, approximately 30 m high, where unweathered high-quality volcanic rocks of QRT are exposed. In this area the thickness of the volcanic rocks is about 45 m, as revealed by a drilling log (GS4 in Figure 1a) executed during the landslide investigation. Progressing downslope, towards the E-NE, the volcanic rocks are deeply weathered, with outcrops consisting of corestones embedded within sandy saprolite. The thickness of this QRT facies progressively reduces downslope, transitioning to SIL near a secondary landslide escarpment. The interpretation of borehole data allow us to infer that the contact between the QRT and SIL formations represents a mechanical weakness zone where landslide failure processes occur.

3 Materials and methods

The measuring system takes advantage of multiple geodetic tools, primarily GNSS and RTS, to track ground displacement of slopes over time.

3.1 GNSS

The GNSS network consists of two permanent GNSS stations (ABB2 and REME, Figure 1) operating in continuous mode and 16 survey-style stations measured periodically from 2019 to 2022. Survey-style stations were measured in long static mode [18] using six dual-frequency (L1 & L2) Topcon Hiper_SR geodetic receivers, which collected data from multiple constellations (GPS and GLONASS). Initially, during the first five survey campaigns, 1.5-h GNSS sessions were conducted. However, post-processing revealed suboptimal ambiguity resolution and increased positional uncertainties, particularly for longer baselines. To enhance measurement quality, we extended the observation period to 2 h, which resulted in improved ambiguity resolution and positional stability for each survey campaign, ultimately leading to more accurate displacement estimates. This duration was selected as an optimal balance between data quality and fieldwork efficiency, accounting for factors such as terrain complexity, sky visibility, and baseline accuracy. To maximize network redundancy and spatial coverage, a strategic station occupation plan was employed. In order to establish a consistent reference framework, the survey-style station G2 was continuously occupied throughout the survey periods, ensuring long acquisition durations near other survey-style stations. Additionally, the GNSS permanent station ESAS, located to the North of the study area, was included in the network. For relative positioning and baseline processing, permanent GNSS stations from the Topcon topnet live network (https://rtk.topnetlive.com/) were selected around the study area (Figure 1b). These stations allow us to obtain a robust regional-scale reference framework for accurate positioning and baseline estimates. The GNSS data underwent an independent post-processing strategy [19] based on the determination of a set of baselines, corresponding to the 3D distance between network elements. The network processing strategy was designed by considering the locations of the stations and the availability of data to ensure maximum precision and robustness. To address the challenges posed by long baselines and the observation durations in survey-style campaigns as above described, a two-stage network processing strategy was employed. The first-order network connects all permanent stations and the survey-style station G2, providing a robust reference framework. The second-order network is made up of shorter baselines within landslide-affected zones, including periodic survey-style stations and the first-order reference stations REME, ABB2, and ESAS. Baseline processing was performed using Leica Infinity v3.4.0 software and precise ephemeris from NASA CDDIS (https://cddis.nasa.gov/Data_and_Derived_Products/GNSS/broadcast_ephemeris_data.html), resolving L1/L2 ambiguities. The FIOR station (Figure 1) was selected as

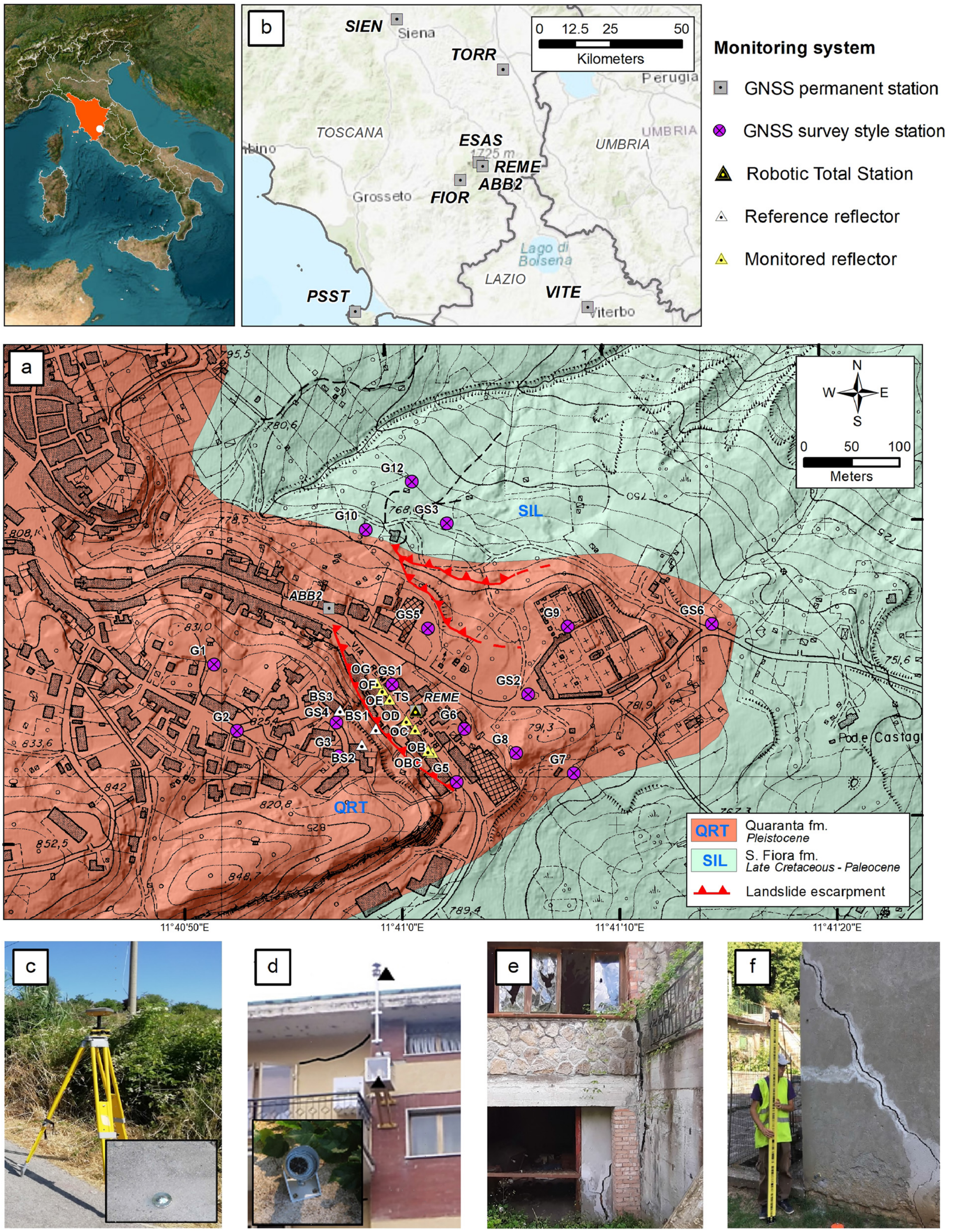

Figure 1: Study area map showing the monitoring network: (a) geology of the study area South of the Abbadia San Salvatore town (modified after [17]) and location of the network elements (grey square: GNSS permanent station; magenta dot: GNSS survey-style station; black triangle: RTS; white triangle: reference reflector for RTS; yellow triangle: monitored reflector); (b) selected Topcon topnet live GNSS permanent stations located around the study area; (c) example of GNSS survey-style station setup; (d) the REME station and RTS installation along with an example of reflector; (e) and (f) building damages caused by landslide displacement.

the fixed reference point for network adjustment [20] as it is the closest to the study area. Redundant observations allowed us to improve outputs reliability by identifying and excluding baselines with higher errors. The final output consisted of a set of multi-temporal ETRF2000 3D coordinates with their respective adjustment corrections (δ), the latter being useful for assessing the precision of the estimates.

3.2 Statistical analysis

Regression is a widely used method for time series analysis and modelling GNSS data to estimate displacement trends [21]. Ordinary Least Square (OLS) regression assumes equal weighting for all observations [22], which can lead to inaccuracies when dealing with sets of GNSS data affected by different δ values. OLS minimises the sum of squared residuals without considering observations quality. As a result, observations with high uncertainties can disproportionately influence the regression fit, skewing velocity estimates and inflating or underestimating displacement trends. To address these limitations, particularly in low signal-to-noise ratio (SNR) cases, Weighted Linear Regression (WLR) was applied to incorporate δ into the model. WLR extends OLS by assigning weights to each observation based on its quality, with smaller uncertainties receiving higher weights [23]. This approach ensures the regression fit is dominated by higher-quality data. To evaluate the stability of the WLR regression fit, 95 % Confidence Interval (CI) calculations [24] were implemented for the predicted displacement values. CIs quantify the range within which the true displacement values are expected to lie. CI analysis was also applied to other contexts related to the modelling of natural phenomena, like shoreline evolution [25], in order to define the uncertainty of shoreline advancement/retreat velocity estimates.

3.3 Robotic Total Station (RTS)

An RTS Topcon DS 101 series, installed close beneath the REME GNSS station, monitors the displacements of a set of selected buildings affected by the landslide. In order to ensure temporal coherence, RTS orientation and coordinates are recalibrated before each measurement cycle using reference reflectors (BS1, BS2, and BS3, Figure 1a) located on stable bedrock within its line of sight (LOS). The RTS is programmed to perform automatic periodic measurements every 3 h. During each cycle, inclined distance, horizontal angle, and vertical angle data are measured for the reflectors installed on selected buildings. Initially configured in a local reference system (x', y', Z), RTS coordinates are later transformed using axis rotation around vertical axis Z, to ensure compatibility with GNSS and InSAR datasets.

3.4 InSAR

The InSAR dataset used in this study was obtained from a public portal [26]. The Persistent Scatterer Interferometry (PSI) data provided were processed using the Sentinel-1A, 1B SAR data and SqueeSAR PSI approach [27]. The dataset includes both ascending and descending geometries for the period 2019 to 2022. The number and spatial distribution of Persistent Scatterers (PS) vary across the study area, with an average density of approximately 1,250 PS/km^2. Higher PS densities (Figure 2) characterize infrastructure-rich regions, while vegetated areas exhibit no PS due to decorrelation effects. Ascending LOS data (Figure 2) revealed displacement patterns along Via Remedi and downslope (East) of the study area, with mean velocities ranging from −4 mm/year to −8 mm/year. In descending geometry, these displacements are not recorded, with most PS exhibiting mean velocities within ±2 mm/year. This indicates that the slope movements are primarily oriented away from the satellite in the ascending geometry. Instead, the area above the volcanic rock main escarpment uphill of Via Remedi showed stable conditions with negligible velocities. Mean LOS velocities were decomposed into East-West and Vertical (V) components by using satellites heading and incident angles known from the literature [28], assuming nil the North-South component. This approach enabled us to complement GNSS and RTS measurements. These datasets provided insights into wider-scale displacement trends and validated the results obtained from ground-based methods.

4 Results

The monitoring system employed in this study provided insights into the state of activity and dynamics of the landslide area located to the South of the Abbadia San Salvatore town. The joint exploitation of GNSS, RTS, and InSAR measurements allowed us to obtain a robust framework for analysing displacement trends.

4.1 GNSS

The GNSS data provided valuable insights into displacement trends. While the SNR in the planimetric components was relatively high, providing precise and accurate velocity estimates, the vertical component exhibited lower quality due to higher noise levels. As a result, the analysis primarily focuses on planimetric displacements. Over the study

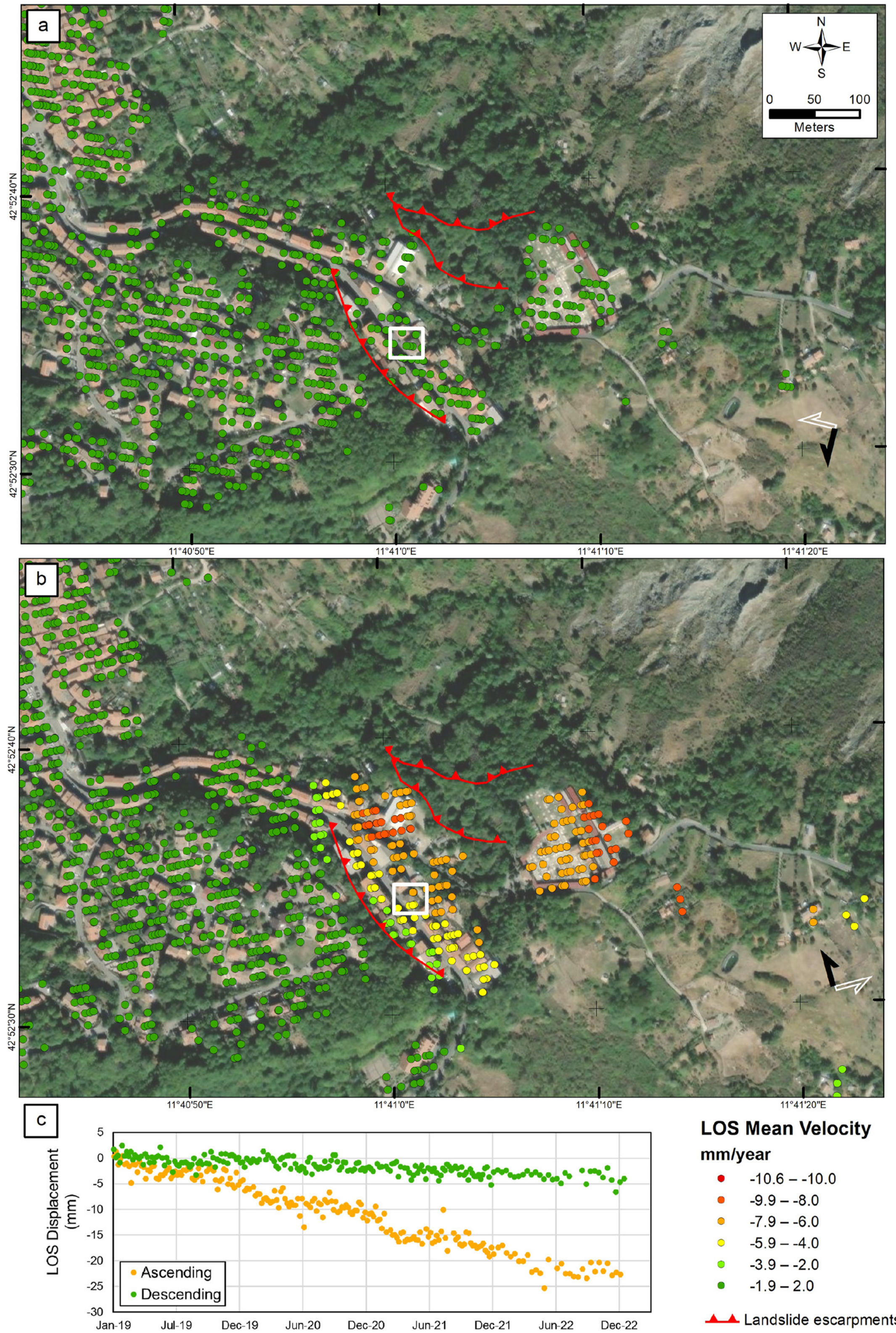

Figure 2: Maps of InSAR LOS velocity for descending (a) and ascending (b) geometries, with black arrows indicating the orbit path and white arrows representing the LOS direction; (c) time series of PS ([26]), located on the building (marked in white) where the RTS is installed.

period, 12 measurement campaigns were conducted, and, for each campaign, the redundancy of the adjusted network is detailed in Table 1. However, post-processing allowed us to use fewer solutions than 12 for certain stations (n in Table 2). Higher adjustment corrections δ were obtained for the first five campaigns, which may be mainly attributed to the shorter 1.5-h observation sessions used during these surveys. The transition to 2-h sessions contributed in fact to improved ambiguity resolution and positioning stability, although other factors such as atmospheric conditions, sky visibility, and baseline geometry may also have influenced these results. Time series obtained for a representative subset of GNSS stations are represented in Figure 3. Velocities in the Easting (V_E) and Northing (V_N) directions estimated using WLR, along with their uncertainties derived from 95 % CIs are detailed in Table 2. To further analyse station displacement characters, V_E and V_N were combined to calculate the planimetric velocity VP and its corresponding azimuth θ for unstable stations (Table 3). This alternative representation of the velocity allowed us to highlight the trend of the planimetric component of the landslide displacement and to compare it with the local morphological pattern. WLR and CI analysis were effective for obtaining more precise and accurate velocity estimates (Figure 3). Stations G1, G2, GS4, and G3 located in the stable area above the volcanic rock escarpment uphill Via Remedi, demonstrated the effectiveness of the implemented methods. For example, G2 showed V_P of *ca.* 3 mm/year using OLS regression, while applying WLR V_P resulted to be around zero, confirming stability with uncertainty of ±2 mm/year for V_E and V_N based on 95 % CI. Similarly, GS4 and G1 confirmed the stability of the underlying bedrock relative to the reference station FIOR. Station G3, located near a East-West trending lineament close to the edge of the volcanic rock escarpment uphill Via Remedi, recorded instead V_E of 4 mm/year ±2 mm/year, but higher uncertainty for V_N, so making right now uncertain the interpretation of these velocity results. Further measurements will provide better velocity estimates for this station. Most stations, except for GS1 and GS3, had average uncertainty of ±2 mm/year, indicating high SNR. Continuous stations REME and ABB2 showed high quality results, with even narrower confidence intervals (±1–2 mm/year). Station GS1 showed V_N of 9 mm/year ± 3 mm/year and V_E 7 mm/year ± 14 mm/year, the latter estimate likely due to multipath errors caused by its proximity to buildings. GS3, the fastest moving station, exhibited velocities of *ca.* 35 mm/year (V_E) and *ca.* 100 mm/year (V_N) with uncertainties of ±27 mm/year and ±17 mm/year respectively. Nevertheless, GS3 trends show marked nonlinear pattern, probably related to seasonal behavior of landslides activity (Figure 3). In these cases both OLS and WLR may fail to model accurately the real landslide kinematics if interpolation is performed over multi-seasonal time periods. To address this issue, a piecewise analysis of the seasonal trend was performed in order to estimate maximum and minimum velocities resulting from nonlinearity. This analyses highlight that the periods between July and October are the slowest, exhibiting minimal displacement. In contrast, the periods between April and July represent the fastest phases of movement. The analysis also allowed us to estimate velocities of approximately *ca.* 105 mm/year

Table 1: GNSS campaigns and degree of freedom for the corresponding adjusted networks.

GNSS campaigns	Degree of freedom
19/07/2019 (t_0)	846
08/11/2019 (t_1)	720
10/06/2020 (t_2)	318
17/07/2020 (t_3)	522
18/09/2020 (t_4)	786
19/11/2020 (t_5)	321
05/03/2021 (t_6)	318
16/07/2021 (t_7)	642
14/10/2021 (t_8)	777
27/01/2022 (t_9)	768
10/06/2022 (t_{10})	429
28/10/2022 (t_{11})	516

Table 2: GNSS stations with number of solutions (n), easting (V_E) and northing (V_N) velocities estimated from WLR with their respective 95 % CI.

Station	n	V_E (mm/year)	95 % CI (mm/year)	V_N (mm/year)	95 % CI (mm/year)
G1	11	0	±2	0	±3
G2	12	0	±1	0	±2
G3	11	4	±2	0	±4
GS4	12	1	±2	0	±3
GS1	10	7	±14	9	±3
REME	10	6	±1	9	±1
G6	12	2	±4	12	±2
G5	10	1	±1	5	±2
G8	12	18	±3	−1	±3
G7	11	2	±2	0	±1
ABB2	11	3	±1	5	±1
GS5	12	4	±3	13	±2
GS2	10	7	±2	11	±3
G9	12	5	±2	12	±1.5
GS6	12	14	±2	17	±4
G10	11	6	±3	21	±3
GS3	12	35	±27	99	±17
G12	12	1	±2	7	±2

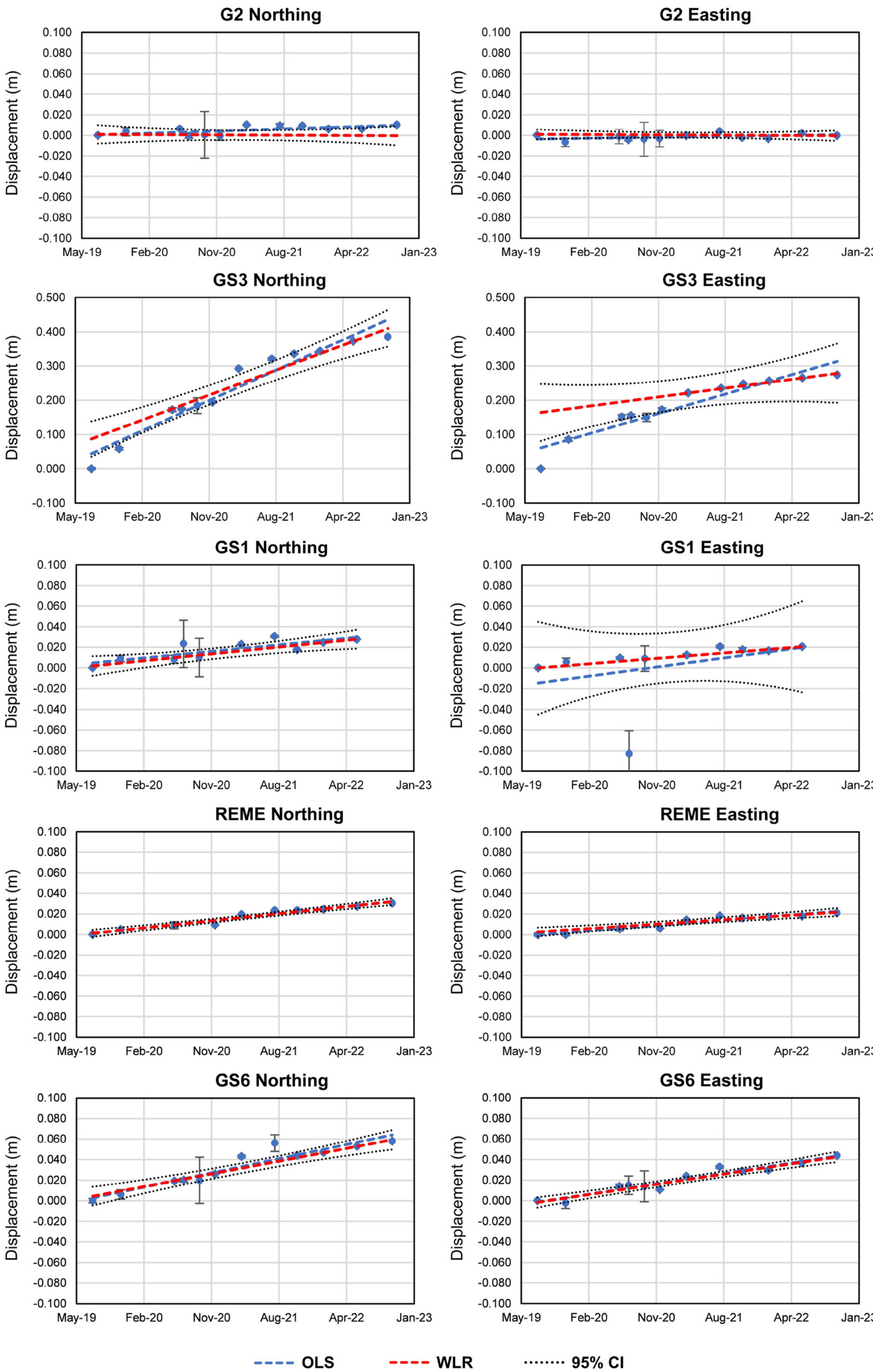

Figure 3: GNSS time series; the blue dots represent the northing and easting displacement components for every campaign relative to the t_0 campaign (Table 1), with their respective adjustment corrections (black error bars); the blue dotted lines indicate the OLS fit, while the red dotted lines represent the WLR fit; the black dotted lines represent the 95 % CI for the WLR fit.

Table 3: Planimetric velocity (V_P) and azimuth (θ) for unstable GNSS stations.

Station	V_P (mm/year)	θ (deg)
G3	4	96
GS1	11	38
REME	11	32
G6	12	351
G5	5	16
G8	19	93
G7	2	105
ABB2	6	33
GS5	13	17
GS2	13	33
G9	13	20
GS6	22	39
G10	21	15
GS3	138	33
G12	7	7

during the fastest periods and *ca.* 35 mm/year during the slowest periods. These results may, in turn, be reasonably linked to rainfall distribution, suggesting a seasonal influence on displacement trends. Overall, the survey style method provided valuable results despite uncertainties at stations with low SNR. It offered a dense network and cost-effective strategy for monitoring where installing continuous GNSS stations was not feasible. The estimated GNSS velocities reflect the long-term displacement trends and, in some cases, non-linear trends of the monitored slow-moving landslide. By applying WLR, high-precision epoch measurements are given more weight, improving the robustness of velocity estimates.

4.2 RTS

The RTS systems provided highly precise "localised" measurements that complemented the GNSS results. Reflectors installed on critical buildings offered insights into both planimetric and vertical displacements. The repeatability of RTS measurements was generally within ±2 mm for both planimetric and vertical coordinates. However, occasional gross deviations were observed during certain measurement cycles and specific targets, likely due to environmental or atmospheric conditions affecting the RTS measurements. These deviations were filtered to obtain representative displacement trends, minimising the impact of significant noise. The average planimetric velocity (V_P) was approximately 8 mm/year, while the vertical velocity (V_V) was around −6 mm/year. Table 4 provides details for the reflectors, including their respective V_P, azimuth (θ)

Table 4: RTS planimetric velocity (V_P) and azimuth (θ), and RTS vertical velocity (V_V) for the monitored reflectors represented in Figure 1.

Reflector	V_P (mm/year)	θ (deg)	V_V (mm/year)
OB	8	19	−6
OBC	5	40	−6
OC	10	47	−7
OD	7	18	−7
OE	7	85	−6
OF	9	56	−5
OG	7	62	−5

and V_V estimates. The reflector OC exhibited larger displacements in both V_P and V_V, while reflectors OC and OD, located at opposite corners of the same building, indicated potential rotational processes. As for V_V, RTS measurements revealed generalised subsidence, in good agreement with landslide activity effects.

5 Discussion

The joint exploitation of GNSS, RTS, and InSAR data enabled a comprehensive ground displacement analysis, providing a deeper understanding of the state of activity and extent of landslide processes in the study area. The velocity data as a whole well correlate with the local geological and geomorphological framework (Figure 1). From GNSS results, stations G1, G2, and GS4 located on the thick unweathered volcanic bedrock, where displacements are near zero, can be considered stable (Figure 4a), in agreement with the InSAR East-West and Vertical components results (Figure 4b and c). This in turn justifies the selection of this area to install the reference reflectors for the RTS measurements. Instead, the reflectors located downhill the volcanic rock main escarpment exhibit planimetric and vertical velocities of 8 mm/year and −7 mm/year respectively, indicating landslide activity in this zone (Figure 4d). GNSS stations REME, GS5, GS2, and G9 show velocity in the order of 15 mm/year, while RTS reflectors located closer to the main escarpment show lower velocities (*ca.* 8 mm/year), suggesting landslide velocity increase toward NE. Notably, the stations GS6 and GS3 experience higher velocity, with GS3 located close downslope the secondary escarpment (Figures 1a and 4a), displaying the highest velocity among all stations. The marked non-linear behaviour of GS3 station may be interpreted as the effect of seasonal, non-uniform distribution of rainfall within the study area. GS6 shows a slight increase in the velocity compared to nearby station G9. This clear

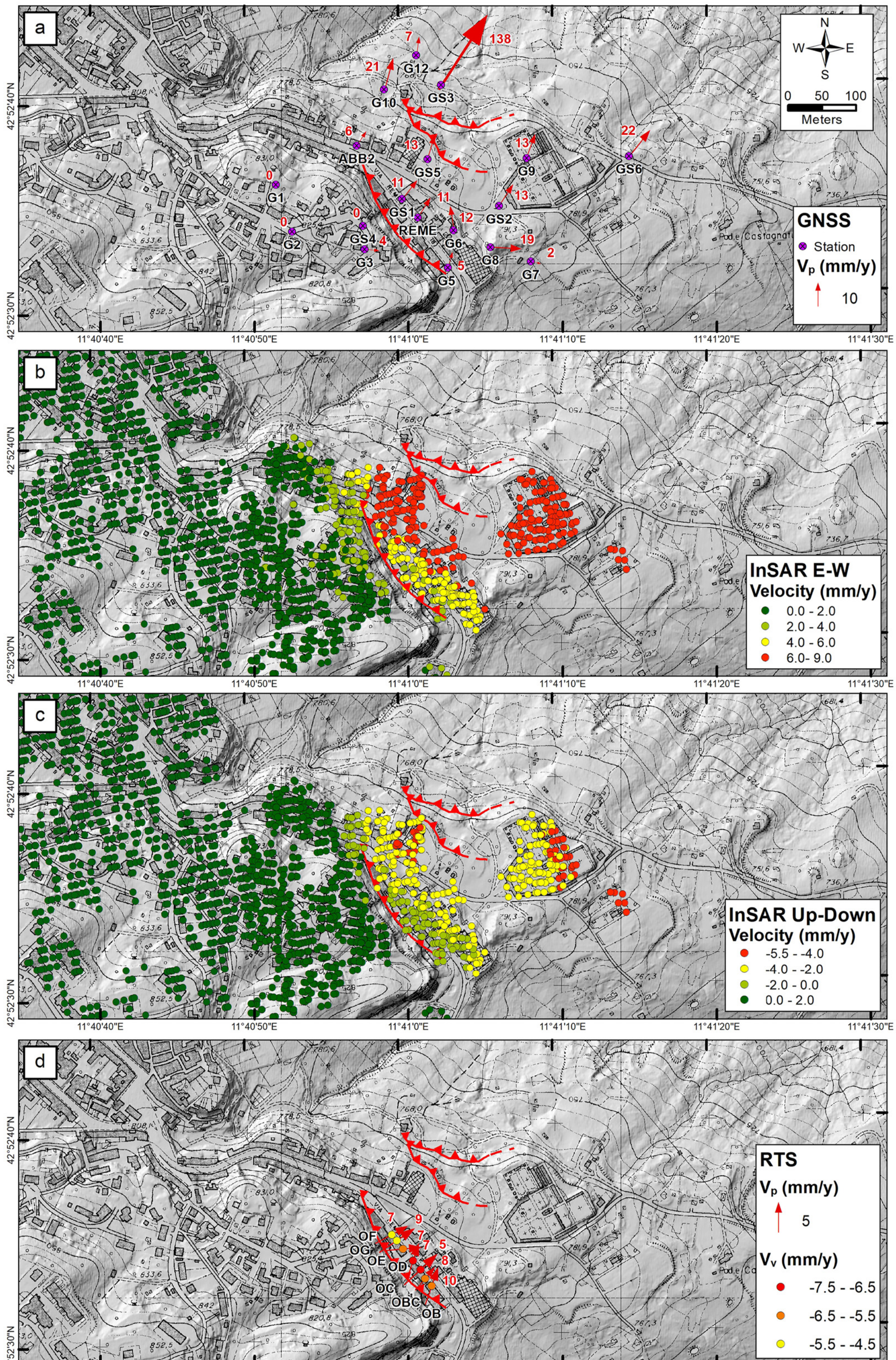

Figure 4: Velocity maps; (a) GNSS; (b) InSAR E-W component; (c) InSAR up-down component; (d) RTS; red line with triangles: landslide escarpment as in Figure 1.

pattern of increased velocity from West to East is evident in both GNSS and InSAR results. On the other hand, the sudden drop in velocity observed between GS3 and G12, both stations being located in the shallowest horizons of the SIL formation, suggests that the landslide rupture surface may daylight in this area. As for θ, almost all the GNSS, RTS and InSAR results for entities located in the active landslide area, show NE-oriented displacement, in good agreement with both local morphology and escarpments trend. When comparing the three systems, GNSS recorded higher velocity rates, whereas InSAR gave slightly lower rates, likely due to LOS sensitivity relative to the true displacement vector. Moreover, projection of InSAR LOS to East-West and Vertical components by ignoring the North-South component introduced uncertainties, as mentioned in [28]. RTS results provided high precision local velocity insights in both planimetric and altimetric directions, information particularly relevant for buildings and infrastructures. However, the distribution of RTS reflectors suffers from limitations caused by reduced visibility due to complex topography. Similarly, InSAR analysis was limited in vegetated areas, where lower PS density led to coverage gaps, with no displacement data available especially in the downhill sector of the study area. As a general outcome, by combining different measuring systems it was possible to provide spatially robust displacement estimates, also allowing for the validation of the reference reflectors for RTS by independent measurements from GNSS and InSAR (at least for E-W and vertical components). The joint exploitation of different systems also offered the capability for analysis at diverse scales, from local (RTS) to large (GNSS and InSAR). Moreover, the multi-source approach allowed us to address the limitations of each measuring system, supporting insights into the dynamics of very slow-moving landslides.

6 Conclusions

This study demonstrates the effectiveness of exploiting together GNSS, RTS, and InSAR for monitoring very slow-moving landslides, by using a case study in the Abbadia San Salvatore town, located on the eastern slope of Mount Amiata, Tuscany, Italy. The proposed multi-source system allowed us to obtain a comprehensive multi-scale ground displacement model, while addressing the challenges and limitations of every measurement system in detecting and estimating very slow displacement trends. For GNSS measurements, SNR limitations prevented accurate estimate of vertical displacement components, while statistical tools such as weighted linear regression and confidence intervals allowed for a more accurate interpretation of horizontal velocity. The survey-style GNSS approach proved to be cost-effective and practical, enabling dense monitoring where installing continuous GNSS stations was unfeasible due to budget constraints or private property restrictions. RTS results provided planimetric and vertical high-precision displacement trends at the building scale. InSAR results available from a public database enabled wider spatial coverage and comparison with ground-based measurements. However, InSAR alone, due to its LOS measurements sensitivity, decorrelation in vegetated areas, and projection limitations, cannot provide a complete picture of the landslide ground displacement field. The results revealed a correlation between displacement patterns and the geological framework, with stable zones corresponding to those areas where unweathered volcanic bedrock is recognized. GNSS and RTS data showed planimetric velocities of *ca.* 10–15 mm/year and vertical velocities reaching −7 mm/year, while InSAR measurements complemented these observations with mean LOS velocities reaching −4 to −8 mm/year in the active landslide zones.

This study contributes to a critical evaluation of precision, accuracy and practical applicability of existing geodetic techniques – survey-style GNSS, RTS, and InSAR – to provide a coherent and comprehensive picture of very slow-moving landslides. By highlighting and comparing their strengths and limitations, we assess the usefulness of these techniques to detect and measure low-magnitude, long-term ground displacements. The results show that, while each technique has certain constraints, their joint use enhances displacement detection and improves spatial resolution, thus ensuring confidence in monitoring outcomes. Finally, the multi-sensor framework here described represents a cost-effective and scalable approach adaptable to other landslide-prone regions, reinforcing the role of geodetic monitoring for landslide hazard assessment and risk mitigation.

Acknowledgments: We thank the Tuscany regional administration, Italy for making the GEOscopio geological database and InSAR data available. Special thanks to those who participated in fieldwork activities, as well as to Fabrizio Piccinelli – Unione dei Comuni Amiata Val d'Orcia and the staff of the Municipality of Abbadia San Salvatore.
Research ethics: Not applicable.
Informed consent: Not applicable.
Author contributions: Conceptualization: L.D.; Data curation: T.V.P.; Formal analysis: L.D., T.V.P. and E.D.; Funding acquisition: L.D. and D.R.; Investigation: T.V.P., L.D., E.D. and D.R.; Methodology: L.D. and T.V.P.; Resources: L.D. and D.R.; Software: T.V.P. and E.D.; Supervision: L.D.; Validation: T.V.P., L.D., E.D. and D.R.; Writing – original draft: T.V.P. and L.D.;

Writing – review and editing: L.D., T.V.P., E.D. and D.R. All authors have accepted responsibility for the entire content of this manuscript and approved its submission.
Use of Large Language Models, AI and Machine Learning Tools: None declared.
Conflict of interest: The authors state no conflict of interest.
Research funding: Financial support was provided by the Scientific Agreement (Accordo di collaborazione scientifica) between the Department of Earth, Environmental and Physical Sciences, University of Siena (resp. L. Disperati), and the Unione dei Comuni Amiata Val d'Orcia.
Data availability: Not applicable.

References

1. Cruden D, Varnes D. Landslide types and processes. In: Turner AK, Schuster RL, editors. Landslides: investigation and mitigation (Special Report 247). Transportation research board, US National Research Council. Washington, D.C.: National Academy Press; 1996:36−75 pp.
2. Lacroix P, Handwerger AL, Bièvre G. Life and death of slow-moving landslides. Nat Rev Earth Environ 2020;1:404−19.
3. Macciotta R, Hendry M, Martin CD. Developing an early warning system for a very slow landslide based on displacement monitoring. Nat Hazards 2016;81:887−907.
4. Stumpf A, Malet JP, Delacourt C. Correlation of satellite image time-series for the detection and monitoring of slow-moving landslides. Rem Sens Environ 2017;189:40−55.
5. Bossi G, Schenato L, Marcato G. Structural health monitoring of a road tunnel intersecting a large and active landslide. Appl Sci 2017;7:1271.
6. González-Arteaga J, Alonso J, Moya M, Merlo O, Navarro V, Yustres Á. Long-term monitoring of the distribution of a building's settlements: sectorization and study of the underlying factors. Eng Struct 2020;205:110111.
7. Corsini A, Castagnetti C, Bertacchini E, Rivola R, Ronchetti F, Capra A. Integrating airborne and multi-temporal long-range terrestrial laser scanning with total station measurements for mapping and monitoring a compound slow moving rock slide. Earth Surf Process Landf 2013;38:1330−8.
8. Colesanti C, Ferretti A, Prati C, Rocca F. Comparing GPS, optical leveling and permanent scatterers. In: IGARSS 2001. Proceedings of the IEEE international geoscience and remote sensing symposium; 2001, vol 6:2622−4 pp.
9. Del Soldato M, Solari L, Raspini F, Bianchini S, Ciampalini A, Montalti R, et al. Monitoring ground instabilities using SAR satellite data: a practical approach. ISPRS Int J GeoInf 2019;8:307.
10. Marroni M, Moratti G, Costantini A, Conticelli S, Benvenuti MG, Pandolfi L, et al. Geology of the Monte Amiata region, southern Tuscany, central Italy. Ital J Geosci 2015;134:171−99.
11. Laurenzi MA, La Felice S. New geochronological data on a core sample from David Lazzaretti well. In: Il vulcano di Monte Amiata. Edizioni Scientifiche e Artistiche; 2017:233−41 pp.
12. Ferrari L, Conticelli S, Burlamacchi L, Manetti P. Volcanological evolution of the Monte Amiata, southern Tuscany: new geological and petrochemical data. Acta Vulcanol 1996;8:41−56.
13. Pavich MJ. Processes and rates of saprolite production and erosion on a foliated granitic rock of the Virginia Piedmont. In: Colman SM, Dethier DP, editors. Rates of chemical weathering of rocks and minerals. London: Academic Press; 1986:551−90 pp.
14. Certini G, Wilson MJ, Hillier SJ, Fraser AR, Delbos E. Mineral weathering in trachydacitic-derived soils and saprolites involving formation of embryonic halloysite and gibbsite at Mt. Amiata, Central Italy. Geoderma 2006;133:173−90.
15. D'Addario E, Giorgetti G, Magrini C, Disperati L. Weathering effects on engineering geological properties of trachydacitic volcanic rocks from the Monte Amiata (Southern Tuscany, Italy). Geosciences 2023;13:299.
16. Coltorti M, Brogi A, Fabbrini L, Firuzabadì D, Pieranni L. The sagging deep-seated gravitational movements on the eastern side of Mt. Amiata (Tuscany, Italy). Nat Hazards 2011;59:191−208.
17. Regione Toscana. GEOscopio - Database Geologico regionale; 2025. Available from: https://www502.regione.toscana.it/geoscopio/geologia.html.
18. Cheloni D, D'Agostino N, D'Anastasio E, Avallone A, Mantenuto S, Giuliani R, et al. Coseismic and initial post-seismic slip of the 2009 Mw 6.3 L'Aquila earthquake, Italy, from GPS measurements. Geophys J Int 2010;181:1539−46.
19. Hofmann-Wellenhof B, Lichtenegger H, Collins J. Global positioning system (GPS) theory and practice. Vienna: Springer; 2001.
20. MOVE3. MOVE3 GNSS baseline processing guide (version 4.6). Sweco Nederland B.V; 2024. Available from: https://move3software.com/downloads/.
21. Gao W, Li Z, Chen Q, Jiang W, Feng Y. Modelling and prediction of GNSS time series using GBDT, LSTM and SVM machine learning approaches. J Geod 2022;96:71.
22. Lee KJ, Wiest MM, Carlin JB. Statistics for clinicians: an introduction to linear regression. J Paediatr Child Health 2014;50:940−3.
23. Suárez E, Pérez CM, Rivera R, Martínez MN. Applications of regression models in epidemiology. Hoboken, New Jersey: Wiley; 2017.
24. Altman DG, Gardner MJ. Calculating confidence intervals for regression and correlation. Br Med J 1988;297:328.
25. Cenci L, Disperati L, Persichillo MG, Oliveira ER, Alves FL, Phillips M. Integrating remote sensing and GIS techniques for monitoring and modeling shoreline evolution to support coastal risk management. GIScience Remote Sens 2018;55:355−75.
26. Regione Toscana. Geoportale Difesa del Suolo - Interferometria SAR satellitare. Geoportale della difesa del suolo della Regione Toscana. Banche dati Difesa del Suolo; 2025. Available from: https://geoportale.lamma.rete.toscana.it/difesa_suolo/#/viewer/326.
27. Ferretti A, Fumagalli A, Novali F, Prati C, Rocca F, Rucci A. A new algorithm for processing interferometric data-stacks: SqueeSAR. IEEE Trans Geosci Rem Sens 2011;49:3460−70.
28. Fuhrmann T, Garthwaite MC. Resolving three-dimensional surface motion with InSAR: constraints from multi-geometry data fusion. Remote Sens 2019;11:241.